

Water vapor changes under global warming and the linkage to present-day interannual variabilities in CMIP5 models

Hanii Takahashi¹ · Hui Su¹ · Jonathan H. Jiang¹

Received: 8 October 2015 / Accepted: 10 February 2016 / Published online: 12 March 2016
© Springer-Verlag Berlin Heidelberg 2016

Abstract The fractional water vapor changes under global warming across 14 Coupled Model Intercomparison Project Phase 5 simulations are analyzed. We show that the mean fractional water vapor changes under global warming in the tropical upper troposphere between 300 and 100 hPa range from 12.4 to 28.0 %/K across all models while the fractional water vapor changes are about 5–8 %/K in other regions and at lower altitudes. The “upper-tropospheric amplification” of the water vapor change is primarily driven by a larger temperature increase in the upper troposphere than in the lower troposphere per degree of surface warming. The relative contributions of atmospheric temperature and relative humidity changes to the water vapor change in each model vary between 71.5 to 131.8 % and 24.8 to –20.1 %, respectively. The inter-model differences in the water vapor change is primarily caused by differences in temperature change, except over the inter-tropical convergence zone within 10°S–10°N where the model differences due to the relative humidity change are significant. Furthermore, we find that there is generally a positive correlation between the rates of water vapor change for long-term surface warming and those on the interannual time scales. However, the rates of water vapor change under long-term warming have a systematic offset from those on the interannual time scales and the dominant contributor to the differences also differs for the two time scales, suggesting caution needs to be taken when inferring long-term water vapor changes from the observed interannual variations.

Keywords Water vapor · CMIP5 · Interannual variations · Climate model · Climate change

1 Introduction

It has long been noted that water vapor is one of the primary contributors to the atmospheric greenhouse effect and is associated with a positive feedback in the climate system (Manabe and Wetherald 1967; Goody and Yung 1989; Randall et al. 2007). Assuming relative humidity (RH) remains unchanged under global warming, water vapor would increase with increasing surface temperature following the Clausius–Clapeyron equation (e.g., Soden and Held 2006). As climate models simulate a reduction of RH in the upper troposphere where radiative fluxes are most sensitive to the water vapor concentration (Udelhofen and Hartmann 1995; Soden et al. 2008), the strength of the water vapor feedback simulated in the climate models is weaker by about 5 % than that computed under the fixed-RH assumption (Soden and Held 2006; Soden et al. 2008). Vial et al. (2013) showed that the inter-model spread in the tropical-averaged water vapor and lapse rate feedbacks can be largely explained by model differences in simulated RH changes; however, the model spreads in the mid-latitudes and polar regions have not been examined. Therefore, decomposing the water vapor changes under global warming into the parts associated with the temperature change and RH change would help the understanding of the factors that control the water vapor feedback and the inter-model spread of feedback strength. The goal of this study is to provide a detailed account of the simulated water vapor changes under global warming in the Coupled Model Intercomparison Project Phase 5 (CMIP5) and a quantification of the relative roles of temperature and RH changes in

✉ Hanii Takahashi
Hanii.Takahashi@jpl.nasa.gov

¹ Jet Propulsion Laboratory, California Institute of Technology, Pasadena, CA, USA

determining the water vapor changes. The decomposition of water vapor change into temperature and RH changes is motivated by the desire to distinguish thermodynamic and dynamic controls of water vapor. Although RH is not a direct prognostic variable in climate models, its variations are strongly tied to model dynamics and physics, including large-scale circulation, convection and cloud microphysics. Such decomposition would help models to isolate deficiencies in order to improve models' representation of water vapor and associated feedbacks.

Jiang et al. (2012) showed that water vapor errors (the differences between simulated and observed water vapor) and the inter-model spread (simulated water vapor differences across models) in the CMIP5 models are the largest in the upper troposphere. In the present-day climate, the CMIP5 models generally have positive water vapor biases in the upper troposphere compared to the Microwave Limb Sounder (MLS) water vapor measurements (Jiang et al. 2012; Takahashi et al. 2015), except over the continental convective regions where negative biases predominate (Takahashi et al. 2015). Takahashi et al. (2015) found that the large errors in the CMIP5-simulated upper tropospheric water vapor (UTWV) are primarily driven by the errors in simulated RH in the troposphere rather than by the temperature errors, except near the tropopause where the temperature and RH errors contribute similarly to the water vapor errors. In this study, we will extend the analysis to water vapor changes in a warmer climate. In addition to separating the contributions of temperature and RH changes to the water vapor changes in each model and their contributions to the inter-model differences, we will also examine how model biases in the present-day climate affect future projections of water vapor.

In this regard, we are interested in the relationship between the water vapor change per degree of surface warming for long-term climate change and the sensitivity on interannual time scales in the current climate. It is well known that the water vapor feedback is strongly positive in all global climate models; however, the magnitude of the water vapor feedback varies between models (Soden and Held 2006). The strength of the water-vapor feedback is primarily determined by the fractional water vapor changes in the tropical upper troposphere (e.g., Dessler and Sherwood 2009). Previous studies used water vapor variations in response to the El Niño-Southern Oscillation (Dessler et al. 2008; Dessler and Wong 2009) or volcanic eruptions (Forster and Collins 2004) to infer the strength of the water-vapor feedback. Dessler et al. (2008) further pointed out that the magnitude of the water vapor feedback could be constant (i.e., independent of the forcing mechanism). Establishing the linkage between present-day climate simulations and quantities associated with long-term climate change is extremely important to constrain model

simulations of climate feedbacks and climate sensitivity (Fasullo and Trenberth 2012; Sherwood et al. 2014; Su et al. 2014; Tian 2015; Zhai et al. 2015). Such analyses will help understand the applicability of interannual variations for long-term climate feedbacks.

The structure of the paper is as follows: Sect. 2 describes the climate model output and the method to decompose water vapor changes; Sect. 3 presents the analysis results; and concluding remarks are given in Sect. 4.

2 Models and methodology

Since the radiative effect of water vapor is roughly proportional to the logarithm of its mixing ratio at a given altitude, the strength of the water-vapor feedback is determined by fractional change of water vapor, rather than absolute change (Soden et al. 2005). Thus, we focus on the fractional water vapor change, i.e., (future-current)/current, in this study. We analyze the patterns and amplitudes of fractional water vapor change in 14 coupled atmospheric-ocean models from the CMIP5 archive (Table 1). The corresponding temperature, RH and cloud fraction changes from these models are also examined. The original simulated monthly model outputs are re-gridded onto the same horizontal grid boxes of 2.5° (longitude) $\times 2^\circ$ (latitude) resolutions for all models.

For the present-day climate, we use the 1980–2004 averages from the historical runs. For the future climate, we use the 2074–2098 averages from the Representative Concentration Pathway (RCP) 4.5 runs (Taylor et al. 2012). The periods are chosen, as all needed variables are available. The RCP 4.5 is a scenario in which projected radiative forcing reaches 4.5 W/m^2 in the year 2100 and stays constant afterwards. It corresponds to the scenario where the CO_2 concentration reaches 538 ppmv in 2100, approximately a doubling of the estimated preindustrial CO_2 concentration of 278 ppmv (Meinshausen et al. 2011). “Climate change” in this study refers to the difference between the future climate and present-day climate; that is, the 25-year averages of 2074–2098 in the RCP 4.5 runs minus the 25-year averages of 1980–2004 in the historical runs: $\Delta(*) = (*)_f - (*)_p$, where the notations f and p refer to the future climate and present-day climate, respectively. For interannual water vapor variations in the current climate (Sect. 3.3), we use the de-seasonalized fractional water vapor ($\frac{WV'}{\overline{WV}}$, where WV' and \overline{WV} indicate de-seasonalized water vapor and climatological water vapor, respectively) from the 25-year historical simulations from 1980 to 2004.

To the first order, water vapor changes follow the global mean surface temperature increase. Table 1 lists the changes in model simulated global-mean air temperature at 2-m height (ΔT_{AS} , near-surface air temperature).

Table 1 Atmosphere-Ocean Coupled CMIP5 models used in this study together with models' equilibrium climate sensitivity (ECS) based on Su et al. (2014) and the corresponding change in global-mean air temperature at 2-m height

Modeling Center	Model Name	Resolution	ΔT_{AS} (K)	ECS (K)
NOAA Geophysical Fluid Dynamics Laboratory, USA	GFDL-cm3	$2.5^\circ \times 2.0^\circ$, L48	3.44	3.97
Met Office Hadley Centre, United Kingdom	UKMO-hadgem2	$1.875^\circ \times 1.25^\circ$, L38	3.38	4.59
Atmosphere and Ocean Research Institute (The University of Tokyo), National Institute for Environmental Studies, and Japan Agency for Marine-Earth Science and Technology	MIROC-esm	$0.56^\circ \times 0.56^\circ$, L56; $1.4^\circ \times 1.4^\circ$, L40	3.06	4.67
Canadian Centre for Climate Modeling and Analysis	CCCMA-canesm2	$2.8125^\circ \times 2.8125^\circ$, L35	2.92	3.69
National Center for Atmospheric Research, USA	NCAR-cam5	$1.25^\circ \times 0.9424^\circ$, L30	2.82	4.1
Institut Pierre-Simon Laplace, France	IPSL-cm5a	$3.75^\circ \times 1.8947^\circ$, L39	2.45	4.13
Commonwealth Scientific and Industrial Research Organization in collaboration with the Queensland Climate Change Centre of Excellence, Australia	CSIRO-mk3.6.0	$1.875^\circ \times 1.875^\circ$, L18	2.43	4.08
Atmosphere and Ocean Research Institute (The University of Tokyo), National Institute for Environmental Studies, and Japan Agency for Marine-Earth Science and Technology	MIROC-miroc5	$0.56^\circ \times 0.56^\circ$, L56; $1.4^\circ \times 1.4^\circ$, L40	2.08	2.72
Centre National de Recherches Meteorologiques/Centre Européen de Recherche et Formation Avancées en Calcul Scientifique, France	CNRM-cm5	$1.4^\circ \times 1.4^\circ$, L31	2.03	3.25
Norwegian Climate Centre	NCC-noresm	$2.5^\circ \times 1.875^\circ$, L26	2.02	2.80
Meteorological Research Institute, Japan	MRI-cgcm3	$1.125^\circ \times 1.121^\circ$, L48	2.02	2.60
Max Planck Institute for Meteorology, Germany	MPI-esm-lr	$1.875^\circ \times 1.875^\circ$, L47	1.85	3.63
NOAA Geophysical Fluid Dynamics Laboratory, USA	GFDL-esm2 g	$2.5^\circ \times 2.0^\circ$, L48	1.14	2.39
NASA Goddard Institute for Space Studies, USA	GISS-e2-r	$2.5^\circ \times 2.0^\circ$, L29	1.09	2.11

ΔT_{AS} ranges from 1.1 to 3.4 K, with a multi-model-mean of 2.3 K. Seven models (GFDL-cm3, UKMO-hadgem-es, MIROC-ecm, CCCMA-canesm2, NCAR-cam5, IPSL-cm5a, CSIRO-mk3.6) have ΔT_{AS} greater than the mean of 2.3 K, and the remaining 7 models (MIROC-miroc5, CNRM-cm5, NCC-noresm, MRI-cgcm3, MPI-esm-lr, GFDL-esm2g, and GISS-e2-r) have ΔT_{AS} less than 2.3 K. The values of ΔT_{AS} are proportional to the models' equilibrium climate sensitivity (Listed in Table 1 of Su et al. 2014). Figure 1 (upper panels) shows the composite zonal-means of fractional water vapor changes for the 7 models with high ΔT_{AS} (>2.3 K) and the 7 models with low ΔT_{AS} (<2.3 K), together with the fractional water vapor changes in each of the 14 models (ordered from higher ΔT_{AS} models to lower ΔT_{AS} models). Although the magnitude of water vapor changes in the high ΔT_{AS} model composite is clearly larger than that in the low ΔT_{AS} model composite, the fractional water vapor change does not monotonically increase with increasing ΔT_{AS} , especially in the upper troposphere (UT). For example, IPSL-cm5a has lower ΔT_{AS} than NCAR-cam5, but the magnitude of UT water vapor changes in IPSL-cm5a is larger than that in NCAR-cam5. MPI-esm-lr has lower ΔT_{AS} but larger fractional UT

water vapor changes than CNRM-cm5, NCC-noresm, and MRI-cgcm3. Therefore, it is worth identifying what other factors drive water vapor changes besides the global-mean surface warming.

The fractional water vapor change normalized by surface temperature $\Delta T_{AS} (\frac{\Delta q}{q_p \times \Delta T_{AS}})$ allows us to examine each model's sensitivity in terms of the water-vapor response to a unit increase of surface temperature, which is more relevant to understanding the model physical processes than using the non-normalized quantities. Figure 1 (lower panels) shows the differences in the zonal-means of normalized fractional water-vapor changes for each model and the composites of high ΔT_{AS} models and low ΔT_{AS} models. The differences in water vapor sensitivity become much smaller after the normalization. However, the pattern and magnitude of fractional water vapor change in each model are still not the same. Hereafter, we focus on the changes normalized by the global-mean ΔT_{AS} unless otherwise stated.

To quantify the relative importance of the fractional water-vapor change due to temperature and that due to RH, we decompose fractional water vapor changes into three terms, similarly to Takahashi et al. (2015):

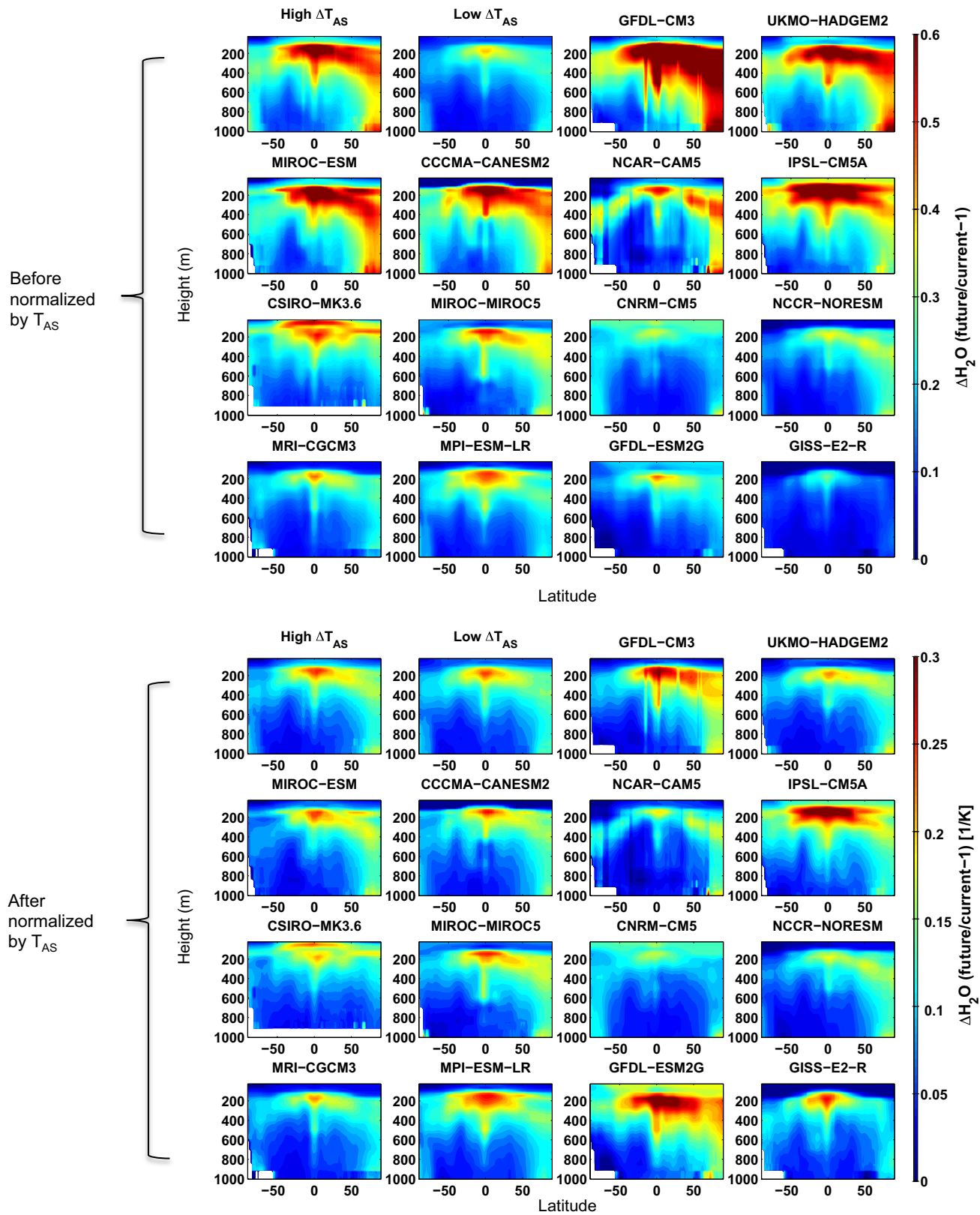


Fig. 1 The composite zonal-mean fractional water vapor changes for the models with high global-mean ΔT_{AS} (>2.3 K) and low global-mean ΔT_{AS} (<2.3 K), together with the zonal-mean fractional water

vapor changes in 14 models (from high to low ΔT_{AS}). *Upper* and *lower panels* represent the water changes before and after the normalization by ΔT_{AS} , respectively

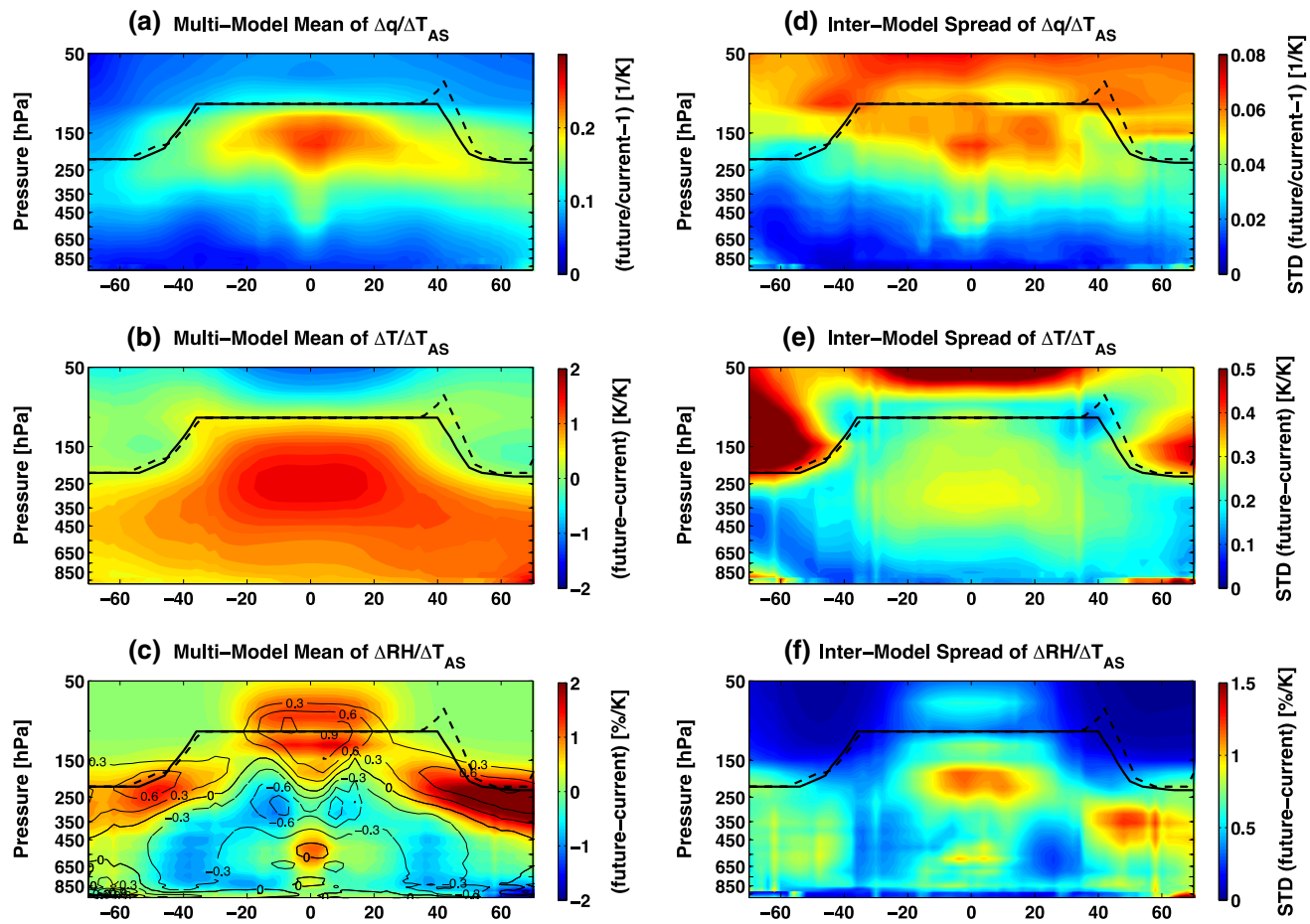


Fig. 2 Latitude-height section of **a** fractional water vapor changes ($\frac{\Delta q}{q_p \Delta T_{AS}}$), **b** temperature changes ($\frac{\Delta T}{\Delta T_{AS}}$), and **c** relative humidity changes ($\frac{\Delta RH}{\Delta T_{AS}}$) averaged over the 14 models (the first column) together with the inter-model spreads (inter-model standard deviations) across

all models (**d–f**, the second column). The changes in cloud fraction ($\frac{\Delta C_{Fr}}{\Delta T_{AS}}$) are shown on the contour plots of RH changes (**c**). The multi-model mean of cold point tropopause in current climate (black lines) and a warmer climate (black-dotted line) are shown over the plots

$$\begin{aligned}
 q &= q_{sat} \cdot RH \\
 \frac{1}{\Delta T_{AS}} \cdot \frac{\Delta q}{q_P} &= \frac{1}{\Delta T_{AS}} \cdot \left\{ \frac{(q_{sat})_P}{q_P} \cdot \Delta RH + \frac{RH_P}{q_P} \cdot \Delta q_{sat} + \frac{\Delta RH \cdot \Delta q_{sat}}{q_P} \right\} \\
 &= \frac{1}{\Delta T_{AS}} \cdot \left\{ \frac{1}{RH_P} \cdot \Delta RH + \frac{1}{(q_{sat})_P} \cdot \Delta q_{sat} + \frac{\Delta RH \cdot \Delta q_{sat}}{q_P} \right\} \\
 &= \Delta q_{RH} + \Delta q_{CC} + \Delta q_{Co-Var} \\
 &= \Delta q_{Tot}
 \end{aligned} \tag{1}$$

where q is specific humidity, $q_{sat}(T)$ is saturation specific humidity (i.e., $q_{sat}(T) = 0.622 \frac{e_s}{P} = 0.622 \frac{10^{9.4041-2354/T}}{P}$), which is a function of temperature and pressure, and RH is the ratio between q and q_{sat} (i.e., $RH = \frac{q}{q_{sat}}$). Δq_{RH} is the normalized fractional water vapor change due to a RH change. Δq_{CC} is the normalized fractional water vapor

change due to a temperature change (approximately governed by the Clausius–Clapeyron relationship) at a pressure level, and the co-variation of these two changes is Δq_{Co-var} .

In Eq. (1), the effects of the present-day mean-state saturation specific humidity (i.e., temperature) and RH can

be seen as a scaling factor for the fractional water vapor changes (by definition). We can further decompose Δq_{RH} and Δq_{CC} into variables in the present-day and under climate change:

$$\ln(\Delta q_{RH}) = \ln\left(\frac{1}{RH_p}\right) + \ln\left(\frac{\Delta RH}{\Delta T_{AS}}\right) = -\ln(RH_p) + \ln\left(\frac{\Delta RH}{\Delta T_{AS}}\right) \quad (2)$$

$$\ln(\Delta q_{CC}) = \ln\left(\frac{1}{(q_{sat})_p}\right) + \ln\left(\frac{\Delta q_{sat}}{\Delta T_{AS}}\right) = -\ln(q_{sat})_p + \ln\left(\frac{\Delta q_{sat}}{\Delta T_{AS}}\right) \quad (3)$$

In this framework, we can quantify the roles of the present-day mean state and future changes of temperature and RH in determining the fractional water vapor changes, which governs the water–vapor feedback in the models.

3 Results

3.1 Latitude-height section of zonal-mean

Figure 2 shows the fractional water vapor changes ($\frac{\Delta q}{q_p \Delta T_{AS}}$), temperature changes ($\frac{\Delta T}{\Delta T_{AS}}$), and relative humidity changes ($\frac{\Delta RH}{\Delta T_{AS}}$) averaged over the 14 models (2a–2c; the first column) together with the inter-model difference (i.e., standard deviation) across all models (2d–2f; the second column). The multi-model-means of the cold-point tropopause (the coldest points in the temperature profiles) in the current climate (solid black lines) and in RCP4.5 (dotted black lines) are marked. The normalized cloud-fraction change ($\frac{\Delta CFr}{\Delta T_{AS}}$) is also shown together with the RH change (black contours in Fig. 2c).

In a warmer world where temperature changes are dominated by anthropogenic factors such as the increases of well-mixed greenhouses gases, temperature increases through the troposphere and decreases in the lower stratosphere (Ramaswamy et al. 2006). RH generally decreases through most of the troposphere, except in the lower and middle troposphere near the equator, and in the upper troposphere and lower stratosphere at all latitudes. The cloud fraction change is highly correlated with the RH change, i.e., regions of increasing RH are associated with increased cloud fraction and vice versa.

The patterns of RH and cloud fraction changes are related to the Hadley Circulation change (Su et al. 2014; Lau and Kim 2015). The rising branch of the climatological Hadley cell between 0° and 5° N/S strengthens under global warming, corresponding to the increased RH there. The weakened upward motion in the convective margins around 5° – 15° N/S leads to decreased RH. The shrinkage of the rising branch of the Hadley cell (so-called

“deep-tropics squeeze” in Lau and Kim 2015) is correlated with the reduced RH over the subtropics (Lau and Kim 2015) and the widening of the subsiding branch of the Hadley cell produces a broadening of the dry zones beyond 40° N/S (Su et al. 2014).

The greater increase of tropospheric temperature with increasing height following the moist adiabat results in large fractional water vapor changes, more than 20 %/K, in the tropical UT above 250 hPa altitude, i.e., an “upper-tropospheric amplification” of water vapor changes. In the lower and middle troposphere, the fractional water–vapor change is about 5–8 %/K. The reduced RH over most of the troposphere counteracts the moistening effect associated with warming.

On the other hand, the largest inter-model differences in water vapor and RH changes are also in the tropical UT above 250 hPa (2d and 2f), where the transition from reduced RH (below 250 hPa in 2c) to increased RH (above 250 hPa in 2c) occurs. For temperature (2e), the largest model differences occur in the lower stratosphere, including both poles, while the tropical UT from 400 to 200 hPa also has relatively large inter-model difference in temperature changes. The largest inter-model difference in RH change occurs around 200 hPa in the tropics and between 450 and 300 hPa in the northern mid-latitudes between 40° and 60° N. The altitudes between 400 hPa and 200 hPa are typically the maximum detrainment levels for deep convection. It is thus reasonable to conjecture that how models treat deep convective detrainment may be related to the inter-model difference in RH changes.

Next, we will disentangle the contributions of temperature and RH changes to the water vapor changes following the methodology described in Sect. 2.

Figure 3 shows the zonal-mean of fractional water vapor change Δq_{Tot} decomposed into Δq_{RH} , Δq_{CC} , and Δq_{Co-var} based on Eq. (1), together with the cold-point tropopause in the current climate (black lines) and in RCP4.5 (black-dotted line). The ratios of tropical (30° S– 30° N) mean $\frac{\Delta q_{RH}}{\Delta q_{Tot}}$, $\frac{\Delta q_{CC}}{\Delta q_{Tot}}$, and $\frac{\Delta q_{Co-var}}{\Delta q_{Tot}}$ at different pressure levels are summarized in column 5 as blue, red, and green lines, respectively.

It is clear that Δq_{Tot} is positive everywhere in most of the models (only CCCMA-canems2 and GISS-r2-r display negative Δq_{Tot} above 100 hPa). The tropical (30° S– 30° N) mean Δq_{Tot} for 100–300, 400–600, and 700–900 hPa ranges from 12.4 to 28.0 %/K, 5.9 to 14.2 %/K, and 3.2 to 7.6 %/K for all models, respectively. This ubiquitous increase in water vapor, especially for 100–300 hPa, is predominantly driven by the universal increase in temperature in the troposphere. In the lower and middle troposphere, the drying effect due to the reduction of RH does not offset the moistening effect associated with the temperature increase, while the cooling of the lower stratosphere does

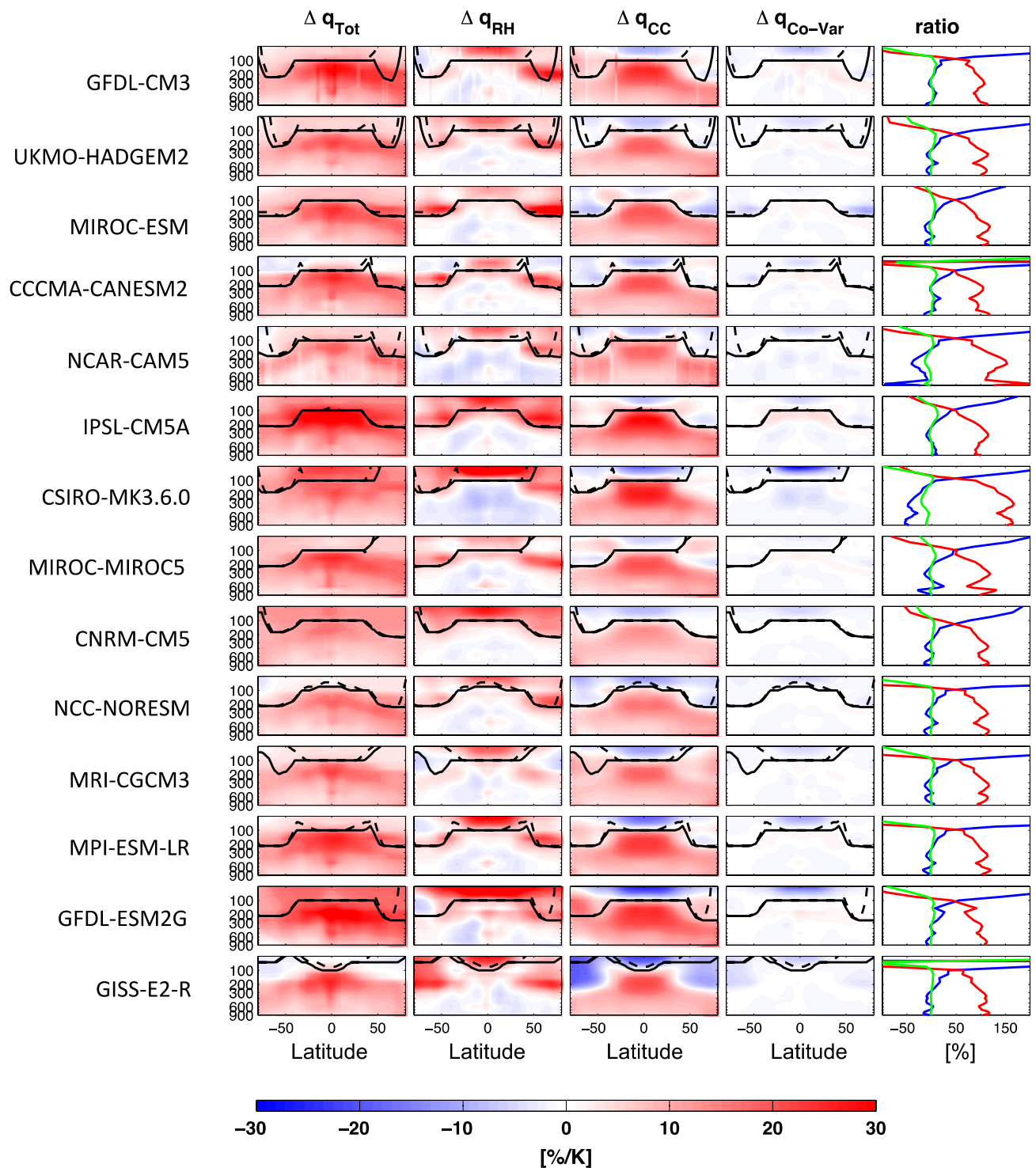


Fig. 3 The zonal-mean of fractional water vapor changes (Δq_{Tot}) decomposed into Δq_{RH} , Δq_{CC} , and $\Delta q_{\text{Co-Var}}$ based on the Eq. (1), together with the cold point tropopause in current climate (black lines) and a warmer climate (black-dotted line) in

each model are shown over the plots (column 1–4). Averaging over all latitudes, the tropical (30°S – 30°N) mean ratios of $\frac{\Delta q_{\text{RH}}}{\Delta q_{\text{Tot}}}$ (blue), $\frac{\Delta q_{\text{CC}}}{\Delta q_{\text{Tot}}}$ (red), and $\frac{\Delta q_{\text{Co-Var}}}{\Delta q_{\text{Tot}}}$ (green) at different pressure levels are also shown (column 5)

not produce a stratospheric drying because the amount of stratospheric water vapor is determined by the coldest temperature (i.e., tropopause temperature) that air parcels

experience along the path into the stratosphere (Fueglistaler et al. 2009) and tends to increase as the climate warms (Minschwaner and Dessler 2004). Coupled with

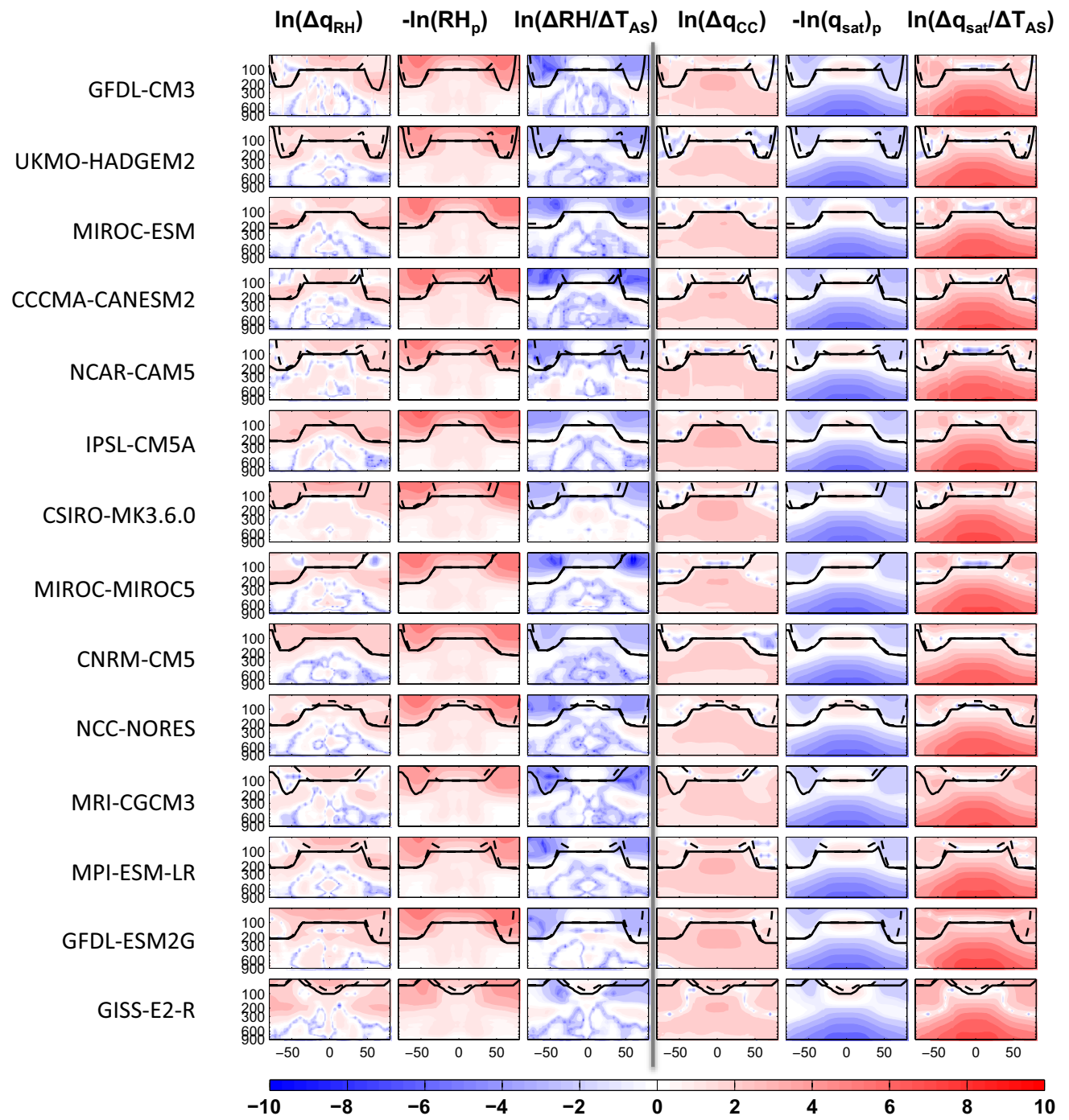


Fig. 4 The zonal-mean of Δq_{RH} decomposed into RH_p and ΔRH_p based on the Eq. (2), and the zonal-mean of Δq_{CC} decomposed into Δ_{satp} and Δq_{sat} based on the Eq. (3)

the decrease of temperature in the lower stratosphere, a strong increase of RH in the lower stratosphere occurs in all models.

Averaging over the tropics (30°S – 30°N), we find that the water vapor change is generally dominated by Δq_{CC} in the troposphere, but the relative contribution of RH increases with height while the temperature contribution

decreases with height. Most models show that Δq_{CC} accounts for 50–125 % and Δq_{RH} accounts for 50 to –25 % of the water–vapor change below the tropopause. Compared to most models, NCAR-cam5 and CSIRO-mk3.6.0 have wider ranges of Δq_{CC} and Δq_{RH} : The percentages of $\Delta q_{CC}(\Delta q_{RH})$ in NCAR-cam5 and CSIRO-mk3.6.0 range between 50 to 200 % (–100 to 50 %) and

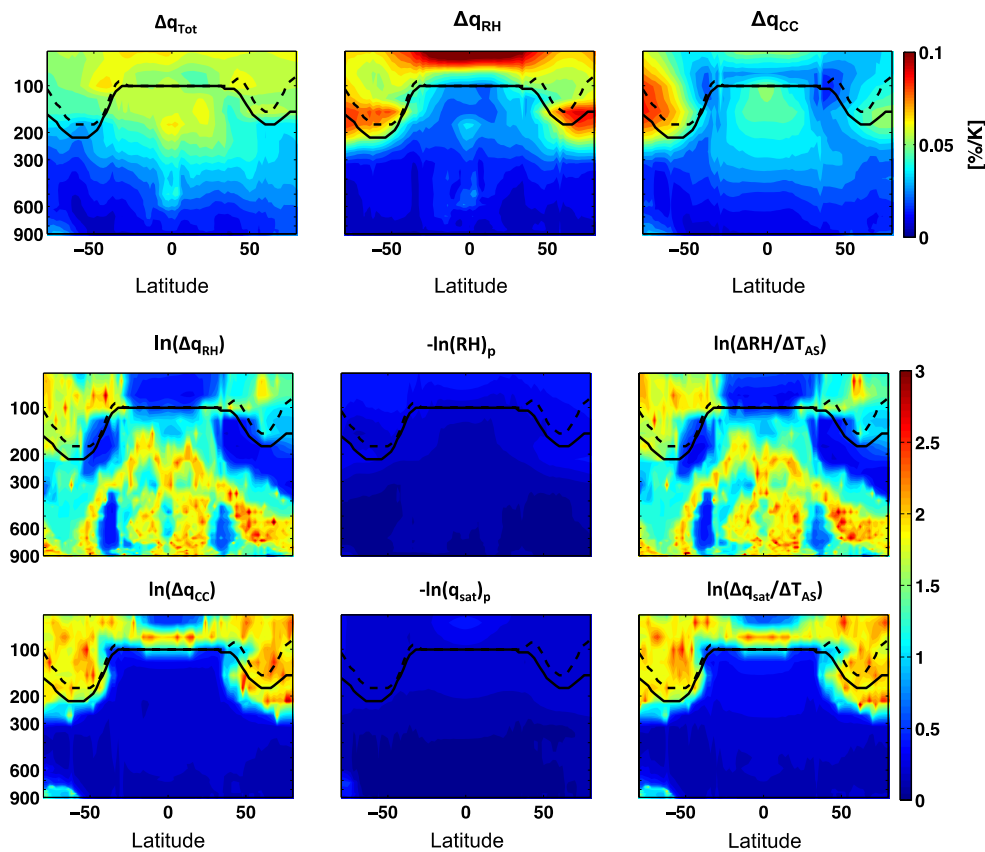


Fig. 5 1st row shows inter-model differences (represented by the standard deviations from the multi-model-mean) in fractional water vapor changes (Δq_{Tot}) together with that of Δq_{RH} and Δq_{CC} . Further,

the inter-model differences of RH_p and ΔRH based on the Eq. (2), and that of Δ_{sat_p} and Δq_{sat} based on the Eq. (3) are shown in 2nd and 3rd row, respectively

50 to 150 % (−50 to 50 %), respectively. The tropical-mean Δq_{CC} and Δq_{RH} contributions averaged between 100 to 300 hPa are between 71.5 to 131.8 % and 24.8 % to −20.1, respectively across the 14 models. The standard deviations of Δq_{CC} and Δq_{RH} are 16.5 and 12.4 %, respectively. Clearly, the models have difficulty in producing a consistent picture of UT water vapor changes. It probably reflects the deficiencies in the models in simulating the impacts of convection on upper tropospheric temperature and RH.

Figure 3 also shows surprisingly large differences in the height of the cold-point tropopause in different models, especially poleward of 40°N/S–45°N/S, where GFDL-cm3, UKMO-hadgem2, CNRM-cm5, and MRI-cgcm3 simulate cold point tropopause height increases with increasing latitude in high latitudes while the rest of models show a decrease in the cold point tropopause height with increasing latitude. GISS-e2r produces a minimum cold point tropopause height at the equator, opposite to all other models. This large discrepancy in the tropopause height suggests a significant discrepancy between CMIP5 models in simulating large-scale dynamics.

Figure 4 shows how the zonal-mean present-day temperature and RH rescale the zonal-mean Δq_{RH} and Δq_{CC} . The spatial variability in Δq_{RH} is clear through the troposphere, and is driven by variability in ΔRH , while Δq_{CC} , T_p , and ΔT are rather uniform from the lower troposphere to the lower stratosphere. The relatively large positive values of Δq_{RH} in the lower stratosphere shown in Figs. 3 and 4 are mainly because of climatologically low RH_p there, permitting a relatively large fractional change. Similarly, the upper tropospheric amplification shown in Δq_{CC} is partly caused by the climatologically low q_{sat_p} associated with the coldest temperature there. This decomposition illustrates that future fractional changes in water vapor depend on present-day water vapor distributions. Model biases in the present-day climate would translate into the errors for future climate changes and climate feedbacks.

Figure 5 (1st row) shows the inter-model differences represented by the standard deviation of model disagreements relative to the multi-model-mean for zonal-mean Δq_{Tot} , Δq_{RH} , and Δq_{CC} . It is clear that the standard deviation of Δq_{RH} across the models is large in the lower stratosphere,

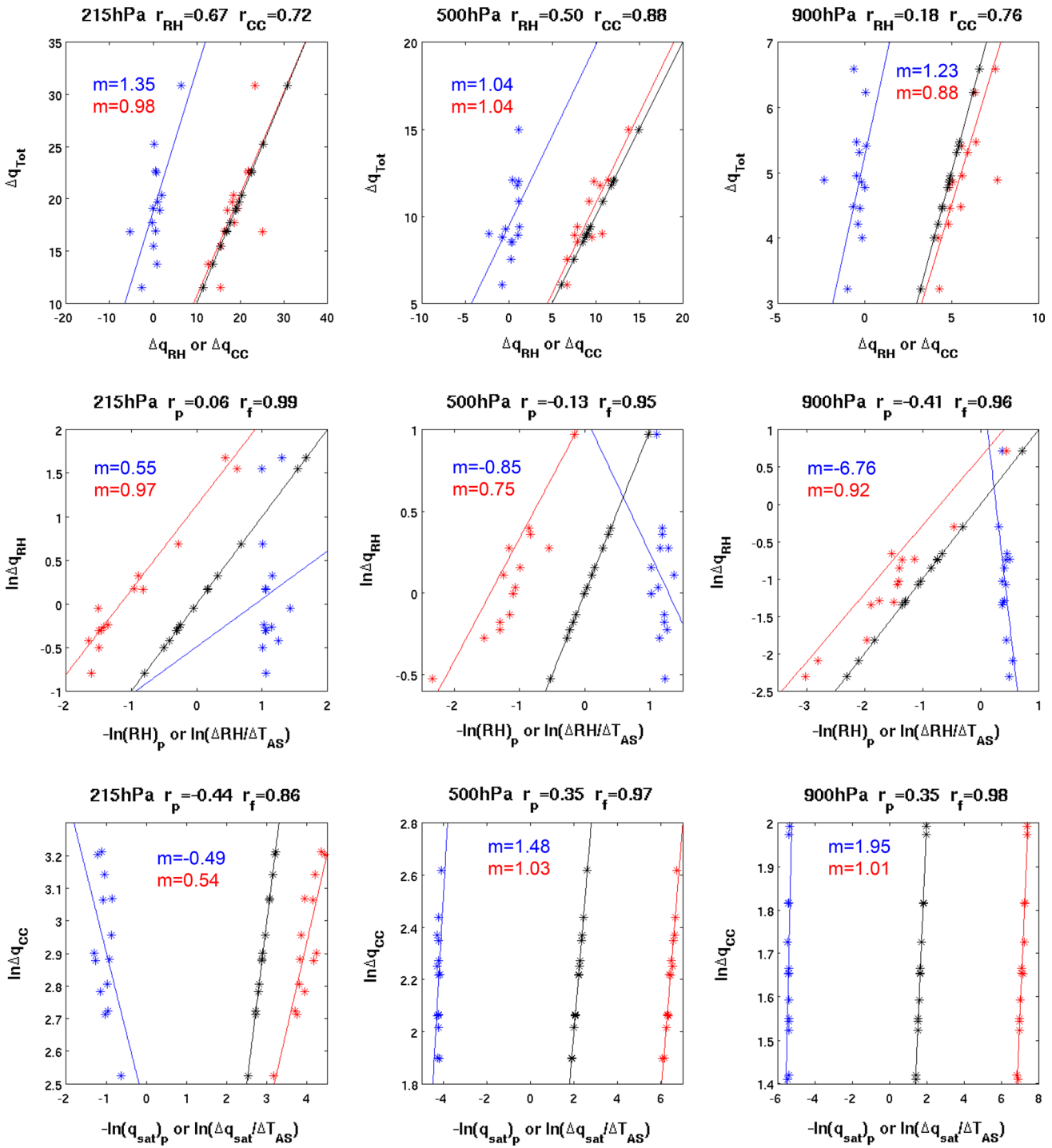


Fig. 6 1st row shows the inter-model relationships between Δq_{tot} versus Δq_{RH} (blue) and Δq_{tot} versus Δq_{CC} (red), 2nd row shows the inter-model relationships between $\ln(\Delta q_{\text{RH}})$ versus $-\ln(RH)_p$ (blue) and $\ln(\Delta q_{\text{RH}})$ versus $\ln(\Delta RH/\Delta T_{\text{AS}})$ (red), and 3rd row shows the inter-model relationships between

$\ln(\Delta q_{\text{CC}})$ versus $-\ln(q_{\text{sat}})_p$ (blue) and $\ln(\Delta q_{\text{CC}})$ versus $\ln(\Delta q_{\text{sat}}/\Delta T_{\text{AS}})$ (red). The black lines are Δq_{tot} versus Δq_{tot} , $\ln(\Delta q_{\text{RH}})$ versus $\ln(\Delta q_{\text{RH}})$, or $\ln(\Delta q_{\text{CC}})$ versus $\ln(\Delta q_{\text{CC}})$ in 1st, 2nd, and 3rd raw, respectively, to show the slope = 1

which highlights the model differences in the stratospheric temperature and water vapor amount. Within the troposphere, the standard deviation of Δq_{RH} is generally smaller

than that of Δq_{CC} , indicating that the simulated temperature differences contribute primarily to the model differences in Δq_{tot} .

To further quantify the contributions of Δq_{RH} and Δq_{CC} to the standard deviation of Δq_{Tot} , we analyze the relationships between the standard deviation in tropical averaged Δq_{Tot} , Δq_{RH} and Δq_{CC} at different pressure levels (215, 500, and 900 hPa). At 215 hPa, Fig. 6 (1st row) shows that the correlation between the standard deviation of Δq_{Tot} and that of Δq_{CC} is 0.72, slightly higher than that the 0.67 between Δq_{Tot} and Δq_{RH} . The regression slope between the standard deviation of Δq_{Tot} versus Δq_{CC} is close to 1 (0.98) and that between Δq_{Tot} versus Δq_{RH} is 1.35, suggesting that the temperature difference has a larger contribution than the RH difference to the water vapor difference across the models.

At 500 hPa, the correlation between Δq_{Tot} and Δq_{CC} (0.88) is much higher than that between Δq_{Tot} and Δq_{RH} (0.50). The slopes between Δq_{Tot} and Δq_{CC} and that between Δq_{Tot} and Δq_{RH} are both 1.04. Again, the standard deviation of Δq_{Tot} is mostly driven by that of Δq_{CC} .

At 900 hPa, the regression slopes of the standard deviation of Δq_{Tot} onto that of Δq_{CC} and Δq_{RH} are 0.88 and 1.23, respectively. While the correlation between Δq_{Tot} and Δq_{CC} (0.76) is high, the correlation between Δq_{Tot} and Δq_{RH} (0.18) is quite low. Therefore, the standard deviation of tropical-mean Δq_{Tot} is mainly due to the standard deviation of Δq_{CC} through the troposphere, except over the equatorial upper troposphere where the inter-model difference in Δq_{RH} is also important.

Similarly, the inter-model differences in zonal-mean $\ln(\Delta q_{RH}) - \ln(RH)_p$ and $\ln(\Delta RH/\Delta T_{AS})$ are shown as the standard deviations from the multi-model-mean in Fig. 5 (2nd row), and the counterparts for $\ln(\Delta q_{CC}) - \ln(q_{sat})_p$ and $\ln(\Delta q_{sat}/\Delta T_{AS})$ shown in Fig. 5 (3rd row). The relationships between the standard deviation of $\ln(\Delta q_{RH})$ versus $-\ln(RH)_p$ and $\ln(\Delta RH/\Delta T_{AS})$, and those of $\ln(\Delta q_{CC})$ versus $-\ln(q_{sat})_p$ and $\ln(\Delta q_{sat}/\Delta T_{AS})$ at different pressure levels are shown in Fig. 6 (2nd and 3rd rows, respectively). There are clear similarities between $\ln(\Delta q_{RH})$ and $\ln(\Delta RH/\Delta T_{AS})$, likewise for $\ln(\Delta q_{CC})$ and $\ln(\Delta q_{sat}/\Delta T_{AS})$ (Fig. 5). As expected, the correlations between the standard deviation of $\ln(\Delta q_{RH})$ and that of $-\ln(RH)_p$ are small for all levels, but the standard deviation of $\ln(\Delta q_{RH})$ is highly correlated with that of $\ln(\Delta q_{sat}/\Delta T_{AS})$ at all levels. Similarly, the standard deviation of $\ln(\Delta q_{CC})$ is highly correlated with that of $\ln(\Delta q_{sat}/\Delta T_{AS})$ for all levels, but not with $-\ln(q_{sat})_p$. These results demonstrate that the standard deviation of Δq_{RH} and Δq_{CC} are caused by the inter-model differences in simulated change under global warming rather than the inter-model differences in present-day simulations.

3.2 Horizontal maps at different pressure levels

Figure 7 shows the multi-model mean of fractional water vapor changes decomposed into each term at different

pressure levels (i.e., 100, 215, 300, 500, and 850 hPa), along with the zonally averaged Δq_{Tot} , Δq_{RH} and Δq_{CC} at different latitudes and different pressure levels (4th column).

As discussed above, the amplitudes of Δq_{CC} account for a larger proportion of Δq_{Tot} than do Δq_{RH} , except at 100 and 215 hPa over 45°–90°N/S, where the relatively larger values of Δq_{RH} are a consequence of the stratospheric cooling.

A substantial moistening in Δq_{Tot} (>20 %/K) can be seen around the inter-tropical convergence zone (ITCZ, 0°–10°S/N and 160°–270°E) in the middle and upper troposphere. The distinctly positive changes around the ITCZ also can be seen in Δq_{RH} . As positive changes in Δq_{CC} are zonally uniform, the strongest moistening of Δq_{Tot} occurs around the ITCZ. From the zonally averaged changes (Fig. 7, 4th column), it is also clear that both Δq_{Tot} and Δq_{RH} have local peaks near the equator, except at 100 hPa. The strong peaks in Δq_{Tot} range between 10 and 20 %/K and those in Δq_{RH} range between 0 and 5 %/K. Although Δq_{RH} makes a smaller contribution to the magnitude of Δq_{Tot} around the ITCZ compared to Δq_{CC} , the spatial pattern of Δq_{Tot} is primarily governed by Δq_{RH} rather than Δq_{CC} .

The roles of Δq_{RH} and Δq_{CC} are further illustrated in Fig. 8, where inter-model standard deviations of Δq_{Tot} , Δq_{RH} , and Δq_{CC} relative to the multi-model-mean at different pressure levels are presented, together with the standard deviations of zonally averaged Δq_{Tot} , Δq_{RH} and Δq_{CC} at different pressure levels (4th column).

Overall, the inter-model differences are smallest at 850 hPa and largest at 100 hPa. At 300 and 500 hPa, both Δq_{Tot} and Δq_{RH} show sizeable model differences over the tropics, especially over the ITCZ. At 500 and 850 hPa, both the magnitudes and patterns of inter-model standard deviations of Δq_{Tot} are largely affected by those of Δq_{RH} rather than Δq_{CC} . At 300 and 215 hPa, both Δq_{CC} and Δq_{RH} are important in determining the inter-model differences in Δq_{Tot} . The model differences at 100 hPa are rather complicated: although the standard deviations of Δq_{Tot} are large over the tropics and subtropics, large model differences are found at high latitudes and subtropics in Δq_{RH} , and large model differences are found at tropics and southern high latitude in Δq_{CC} . Inter-model standard deviations of Δq_{Tot} in tropics are largely affected by those of Δq_{CC} , while those in subtropics are caused by Δq_{RH} .

To quantify the contributions of temperature and RH to the inter-model standard deviations, we also calculated the inter-model relationships between the spreads in Δq_{Tot} and Δq_{RH} and between Δq_{Tot} and Δq_{CC} over the ITCZ, similarly to Fig. 6. At 215 and 300 hPa over the ITCZ, the inter-model correlations between the spreads in Δq_{Tot} and Δq_{RH} are as strong as that between Δq_{Tot} and Δq_{CC} . At 500

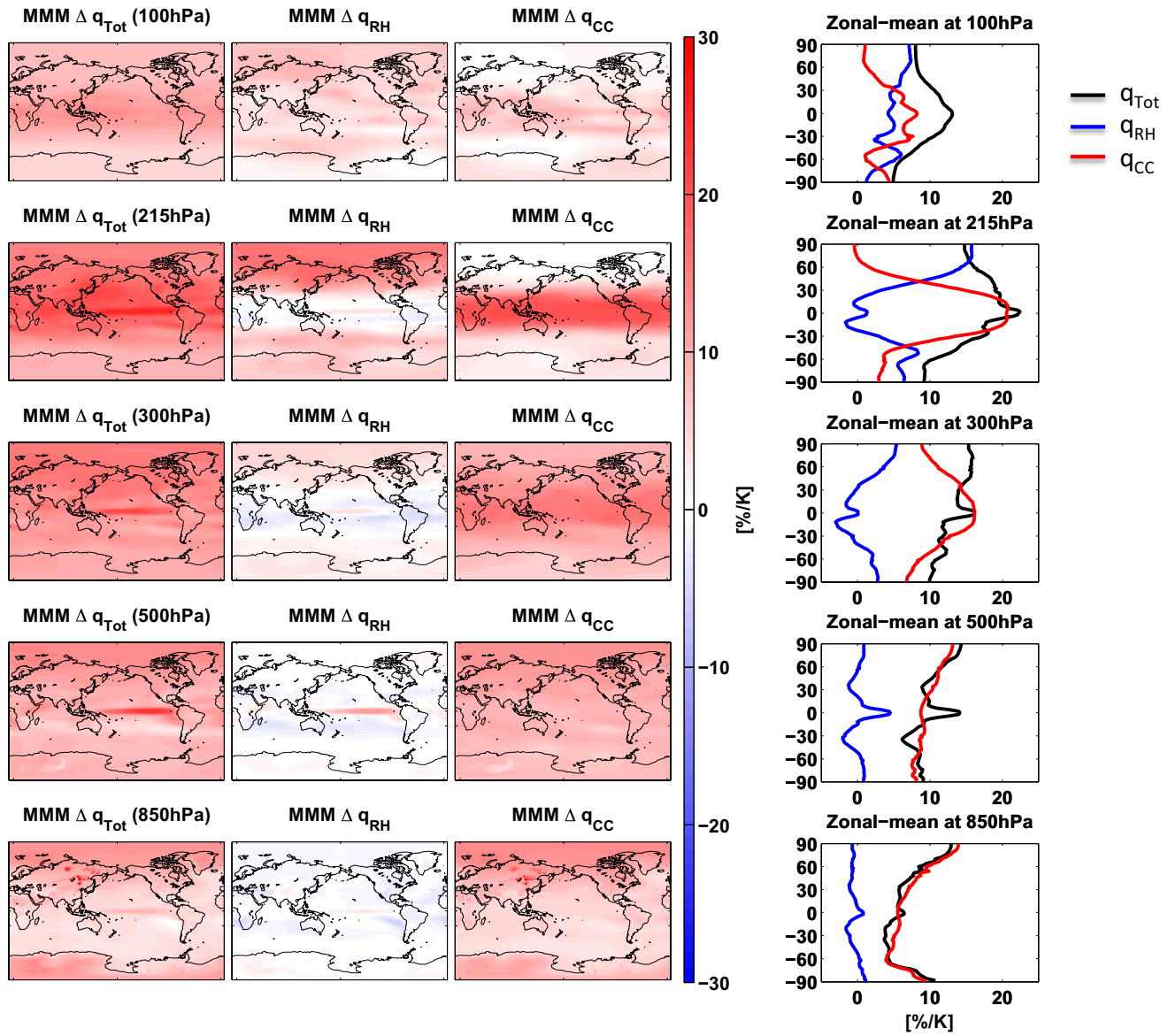


Fig. 7 Global maps of fractional water vapor changes decomposed into each term at different pressure levels (1st to 3rd column), together with the zonally averaged inter-model standard deviations in Δq_{Tot} (black), Δq_{Tot} (blue) and Δq_{CC} (red) at different pressure levels (4th column)

and 850 hPa over the ITCZ, on the other hand, the inter-model correlation between the spreads in Δq_{Tot} and Δq_{RH} is stronger than that between Δq_{Tot} and Δq_{CC} (Figure not shown).

3.3 Water vapor changes under global warming and the linkage to inter-annual variability in present-day climate

Previous studies (Dessler et al. 2008; Dessler and Wong 2009) suggested that the observed interannual variations of water vapor could be used as a proxy to project water vapor feedback under climate change. To find a linkage

between the future climate and current climate, we compare the rates of water vapor change under global warming to the rates of water vapor change with T_{AS} derived from inter-annual variability in the current climate. The rates of water vapor change under global warming are defined as the difference in the averages between 2074 and 2098 (RCP 4.5 runs) and 1980–2004 (historical runs), normalized by tropical-mean or global-mean T_{AS} (i.e., $\frac{\Delta q}{q_p \times \Delta T_{\text{AS}}}$).

Similarly, the rates of q_{sat} and RH changes normalized by T_{AS} under global warming over the tropics and the globe are estimated. We call those rates of water vapor, saturation specific humidity (q_{sat}), and RH as “future rates”.

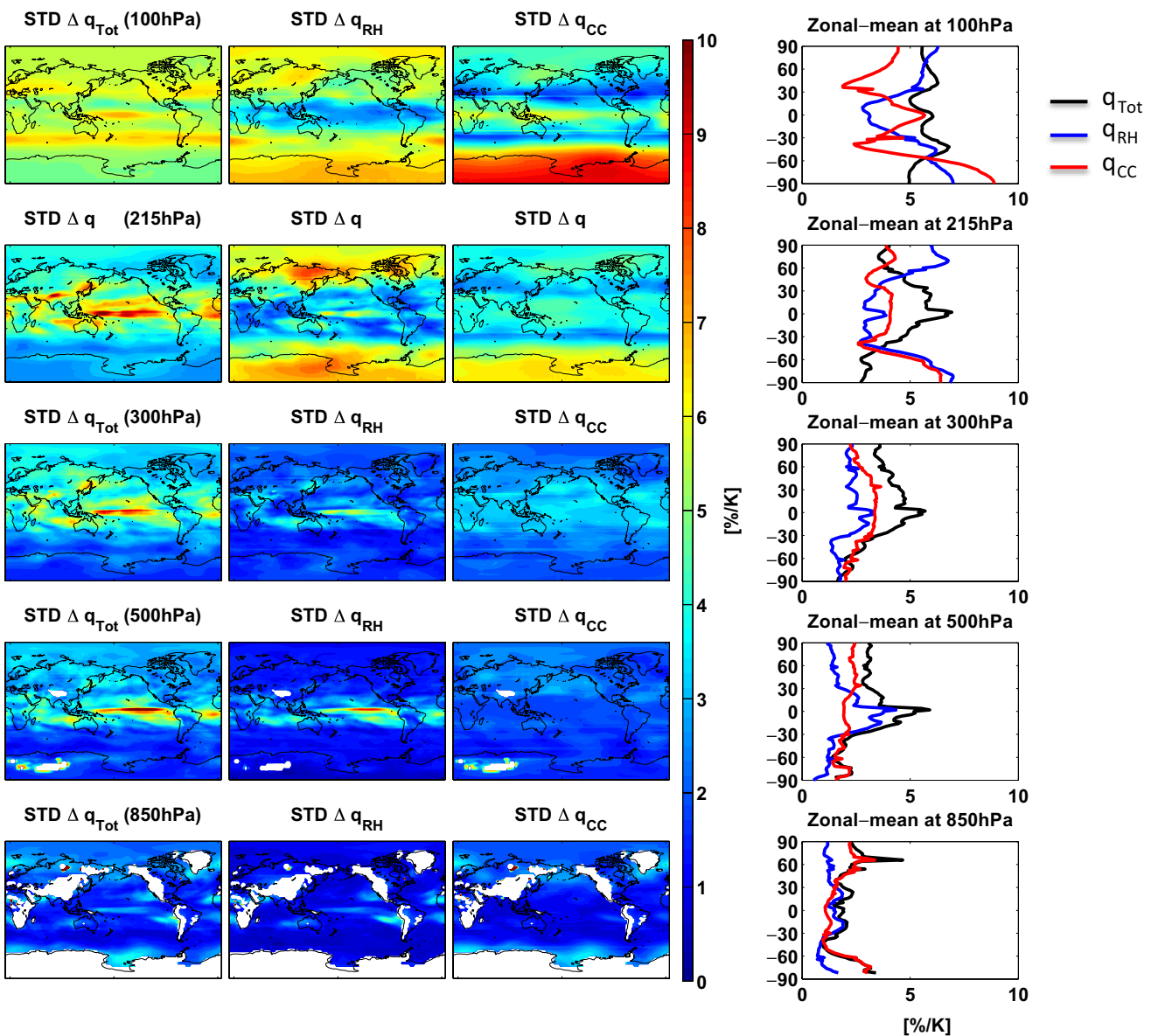


Fig. 8 Global maps of inter-model standard deviations in Δq_{Tot} , Δq_{RH} and Δq_{CC} at different pressure levels (1st to 3rd column), together with the zonally averaged inter-model standard deviations in Δq_{Tot} , Δq_{RH} and Δq_{CC} at different pressure levels (4th column)

On the other hand, the rates of water vapor change with T_{AS} derived from inter-annual variability in the current climate are calculated from the historical runs from 1980 to 2004. The rates of water vapor change computed from inter-annual variability are demonstrated in Fig. 9a, which represents the tropical linear regression between the de-seasonalized fractional water vapor ($\frac{WV'}{WV}$, see Sect. 2) at 215 hPa versus that of de-seasonalized $T_{\text{AS}}(T'_{\text{AS}})$. We find that the correlations between $\frac{WV'}{WV}$ and T'_{AS} are highly positive ($r \geq 0.8$) for all models, except CSIRO-mk3.6.0 ($r = 0.16$) and MRI-cgcm3 ($r = 0.46$). The rates of fractional water vapor changes with T_{AS} vary between 20 and 32 % at 215 hPa, except for CSIRO-mk3.6.0 and

MRI-cgcm3. CSIRO-mk3.6.0 produces a 3.8 % increase in water vapor per degree of T_{AS} increase, while the MRI-cgcm3 shows a 10.7 %/K increase in water vapor. The low water vapor sensitivities in the two models do not originate from the rate of UT temperature increase with T_{AS} (Fig. 9b) as all models show the increase in UT temperature with T_{AS} at a rate about 2.0 K/K on the interannual time scales. Instead, the relatively large decrease of tropospheric RH with surface warming in the two models contributes to the lower water vapor sensitivity (Fig. 10).

For current climate interannual variations, we use the water vapor, q_{sat} or RH changes averaged over the tropics or the globe versus tropical-mean or global-mean surface

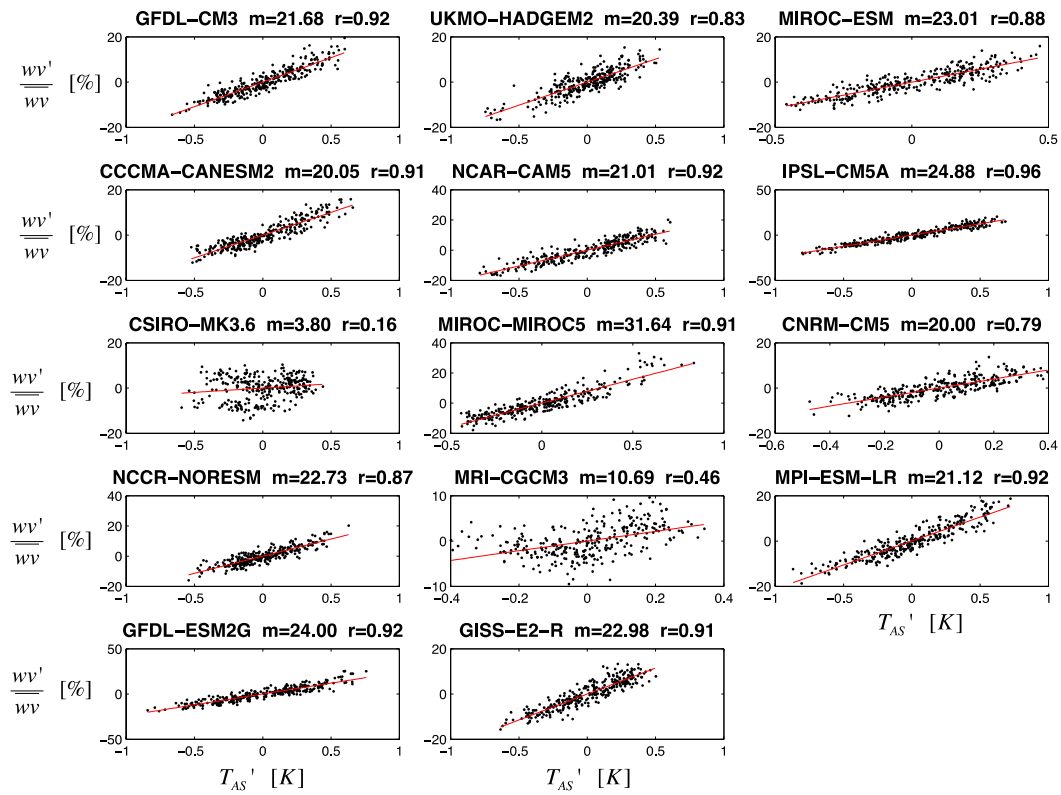
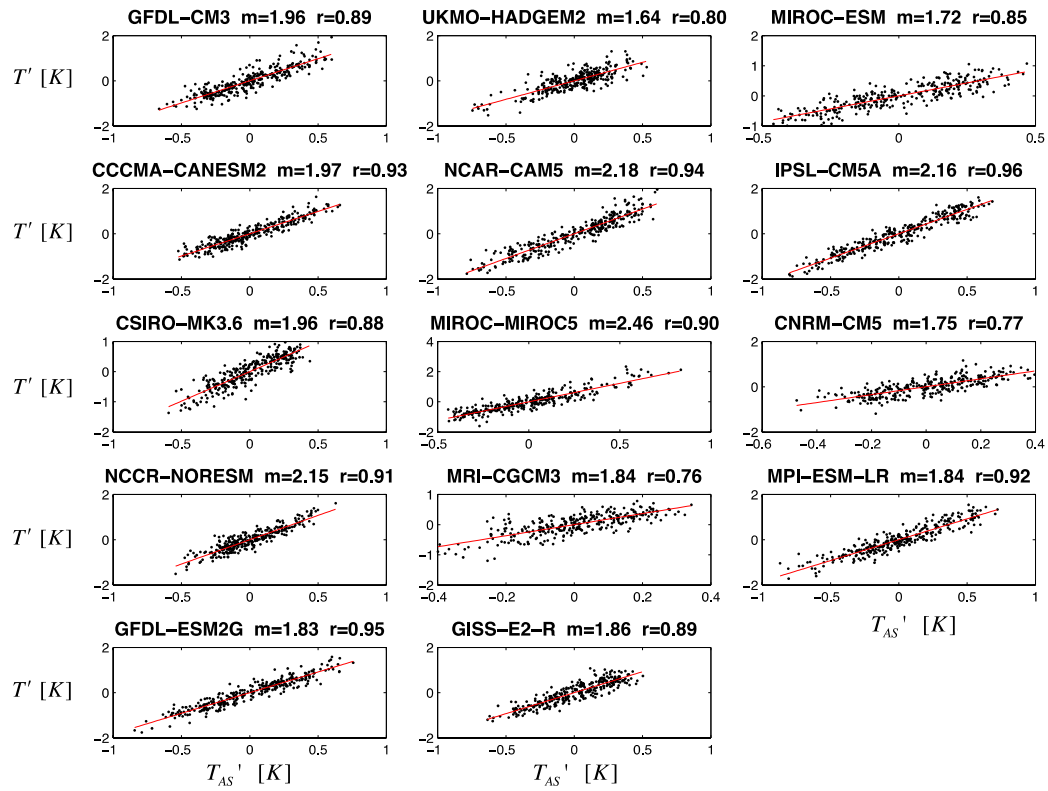
(a) Water Vapor in Current Climate at 215 hPa**(b)** Temperature in Current Climate at 215 hPa

Fig. 9 The linear regression between the tropical inter-annual variability in fractional water at 215 hPa and that in T_{AS} (a), and between the tropical inter-annual variability in fractional temperature at 215 hPa and that in T_{AS} (b)

air temperature, respectively. We call the regression slopes of averaged water vapor, q_{sat} and RH versus T_{AS} as “current rates” in the following discussion.

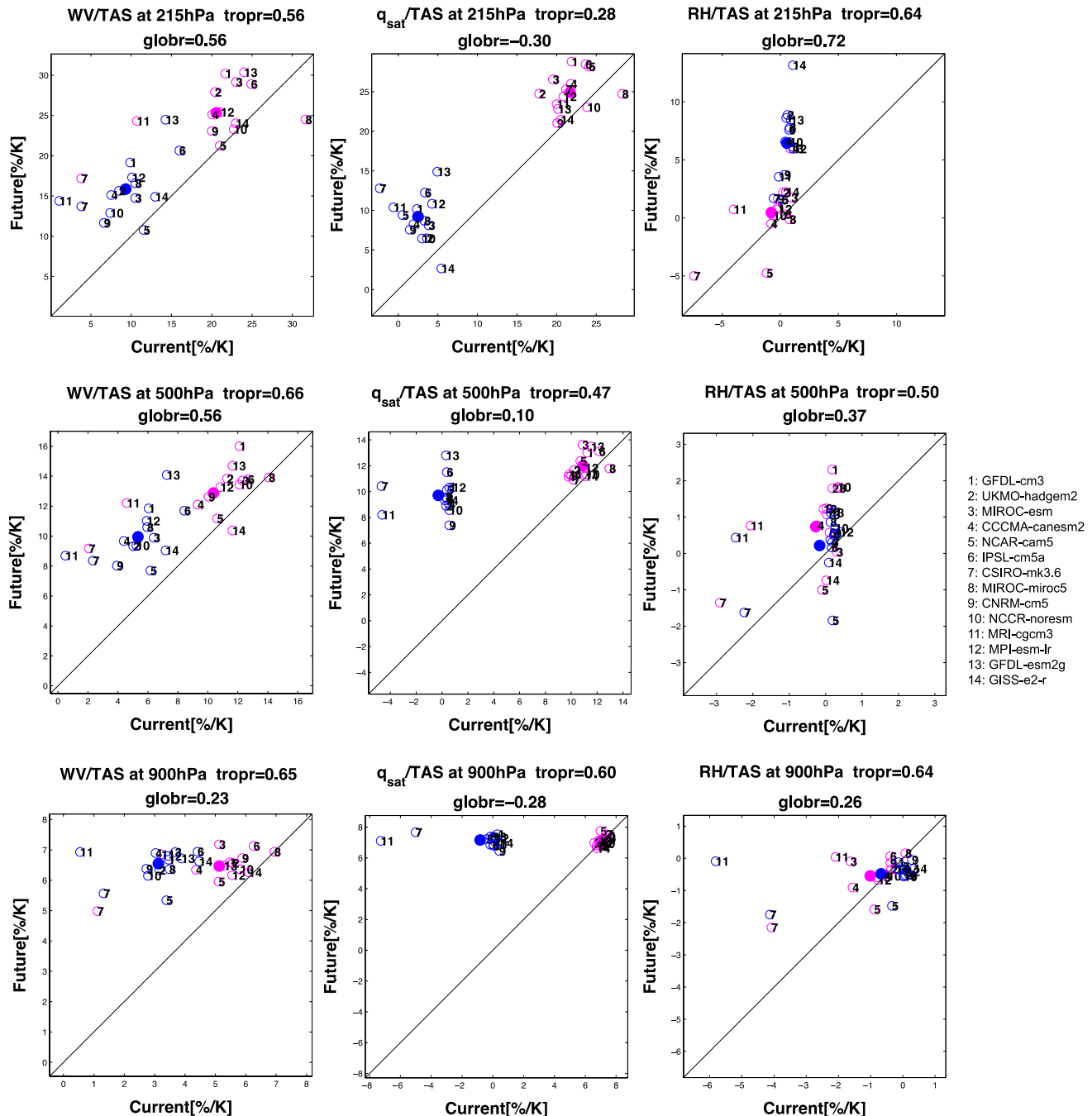


Fig. 10 The relationship between current and future rates in water vapor, q_{sat} , and RH at different pressure levels. The rates in each model over the tropics and over the whole globe are marked as

Figure 10 displays the relationship between *current* and *future rates* in water vapor, q_{sat} , and RH at different pressure levels (i.e., 215, 500, and 900 hPa). The *rates* in each model over the tropics and over the globe are marked as magenta and blue circles respectively. In addition, the ensemble means of the *rates* across all models over the tropics and over the globe are marked as magenta and blue solid circles respectively.

In general, future tropical *rates* in water vapor above the boundary layer are higher than future global *rates*. This is because ΔT_{AS} in mid-and high-latitudes is much larger than that in the tropics under global warming and the average water-vapor changes are dominated by tropical changes. In a similar manner, future tropical *rates* for q_{sat} are also higher than future global *rates*.

For water vapor, it is clear that the current and future *rates* are not equal. Future *rates* are persistently higher than current *rates* over the tropics and over the globe for all models, except for 2–3 models. Note that our definition of future *rates* is the centennial difference between the RCP4.5 and historical runs. It includes rapid adjustment to external forcings and internal feedbacks. Nevertheless, our results indicate that the water vapor changes with T_{AS} derived from present-day inter-annual variability may have a systematic offset relative to those for long-term climate changes.

On the other hand, for water vapor, the inter-model differences in current and future *rates* are correlated. Models that have smaller current *rates* also have smaller future *rates* and vice versa. The correlations between the current and future tropical *rates* are around 0.6 at all levels. For the global averages, the correlations are lower, especially in the lower troposphere. Two models, CSIRO-mk3.6 and MRI-cgcm3 deviate from the rest of models significantly at 500 and 215 hPa. At 900 hPa, future and current *rates* are quite consistent among the models, except for those two models, CSIRO-mk3.6 and MRI-cgcm3, which have noticeably lower current *rates*. It is also worth pointing out that current tropical *rates* have a wider range than future tropical *rates*. For example, for water vapor at 215 hPa, the range of current tropical *rates* (3.8–31.6 %/K) is larger than that of future tropical *rates* (17.2–30.4 %/K). On the other hand, the range of current global *rates* is comparable to that of future global *rates*.

For q_{sat} , the future tropical *rates* are close to the current tropical *rates*, but the future global *rates* are higher than the current global *rates* at all levels. The inter-annual variability in tropical-averaged tropospheric q_{sat} could be used to indicate future changes. Biases may be introduced when the interannual variations of global-averaged tropospheric temperature are used to represent its long-term changes.

For RH, the tropical or global averages on the interannual time scale result from the cancelling effects from different regions and have a rather weak correlation with the averaged T_{AS} (figure not shown). The RH sensitivities to T_{AS} show a rather clustered pattern with most models concentrated near zero, a manifestation of the fixed-RH assumption on large-scale averages. Two models (CSIRO-mk3.6 and MRI-cgcm3) are noticeable outliers: both show significant reduction in the averaged RH with the increasing

of T_{AS} on interannual time scales, which is consistent with their lower water vapor increase with T_{AS} than the other models.

From Figs. 5 and 6, it is seen that the inter-model differences in tropical water vapor rates in the future are mainly controlled by the inter-model differences in temperature rather than RH. Since the inter-model differences in current and future water vapor *rates* are somehow correlated, it is worth testing if the inter-model differences in current water vapor *rates* are also mainly due to the inter-model differences in current temperature *rates* rather than current RH *rates*. Figure 11 shows the inter-model relationships between current water vapor *rates* versus current q_{sat} *rates* (magenta), and current water vapor *rates* versus current RH *rates* (blue) for the tropical (left panel) and global (right panel) averages. This reveals that the contribution of the inter-model differences in current RH *rates* to current water vapor *rates* are actually higher than that of current q_{sat} *rates* to current water vapor *rates*, except at 500 hPa over the globe, where both current q_{sat} *rates* and current RH *rates* contribute to current water vapor *rates*. This result indicates that although the inter-model differences in current and future tropical water vapor *rates* generally have good correlations, it does not mean that the sources of these spreads are the same. Caution needs to be taken when using interannual variations of water vapor as a proxy for water vapor feedback under climate change. Different processes may dominate the inter-model differences in the water vapor changes under long-term climate change and those on the inter-annual time scales.

4 Summary and discussion

This paper investigates water vapor changes in a warmer climate in CMIP5 simulations and links these to simulated climate variability on the interannual time scales in present-day climate. Detailed analyses are performed to quantify how temperature and RH contribute to the water vapor changes and inter-model differences in water vapor changes. To find a link between the future climate and current climate, the rates of water vapor under global warming (future *rates*) are compared to the rates on interannual time scales in historical simulations (current *rates*).

Our results show that the fractional water vapor change is about 5–8 %/K in the lower and middle troposphere in a projected climate change scenario, and more than 20 %/K in the tropical UT above 250 hPa. The tropical-averaged UT water vapor increases range from 12.4 to 28.0 %/K across the 14 models. Averaging over the tropics, the models show that the fractional water vapor change due to temperature changes (Δq_{CC}) accounts for 71.5–131.8 % and the

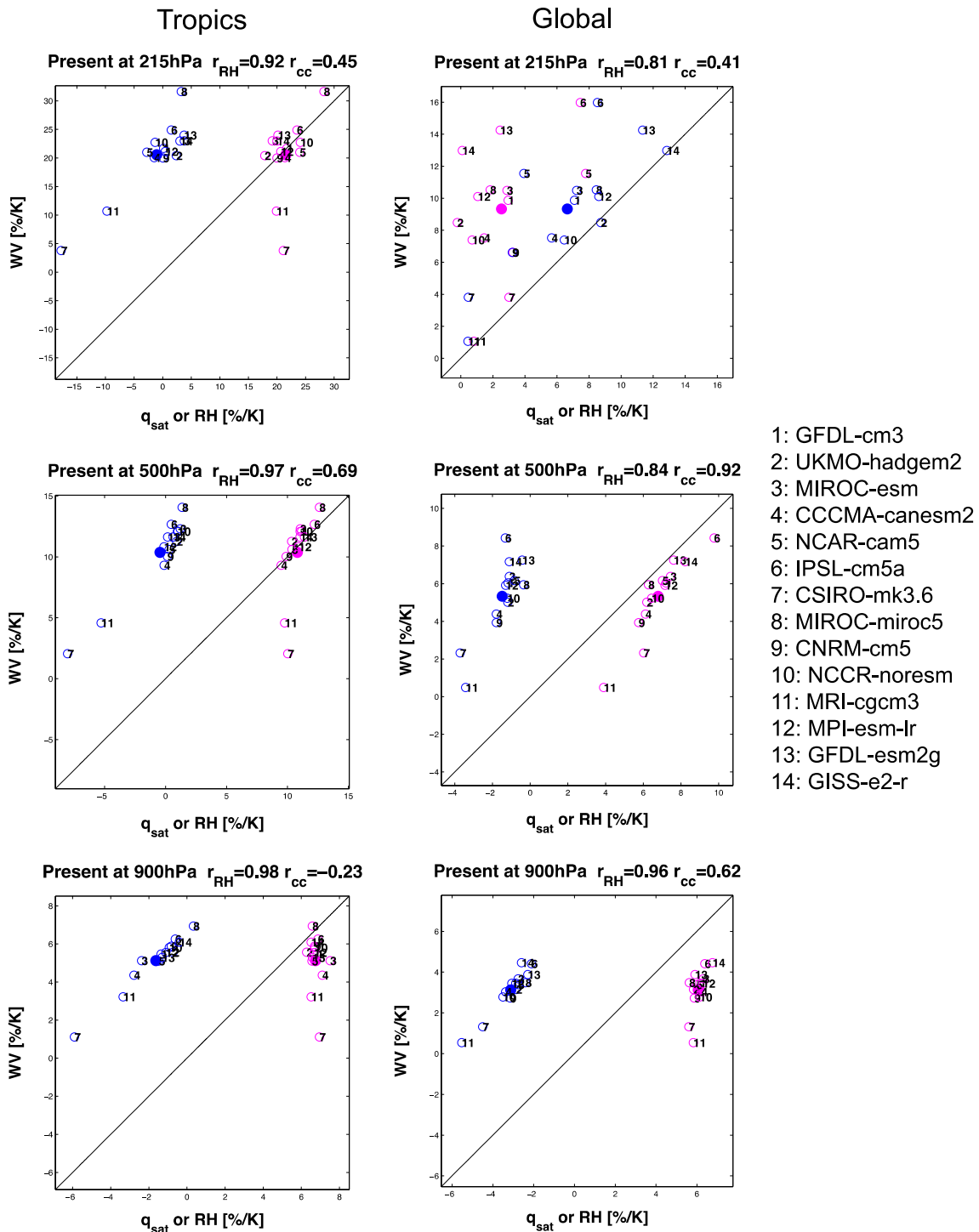


Fig. 11 The inter-model relationships between current water vapor rates versus current q_{sat} rates (magenta), and current water vapor rates versus current RH rates (blue) over the tropics (left) and globe

(right) at different pressure levels. In addition, the ensemble-means across all models are marked as *solid circles*

fractional water vapor change due to RH changes (Δq_{RH}) accounts for -20 to 24.8% . A substantial moistening of Δq_{Tot} ($>20\%/\text{K}$) in the middle and upper troposphere is seen near the ITCZ (0° – 10°S/N and 160°E – 270°E). There,

although Δq_{RH} has a smaller contribution to the magnitude of Δq_{Tot} compared to Δq_{CC} , the pattern of Δq_{Tot} is determined by Δq_{RH} rather than Δq_{CC} because Δq_{CC} is approximately horizontally uniform.

The fractional change of water vapor depends on the present-day water vapor climatology, but the inter-model differences in Δq_{RH} and Δq_{CC} is largely caused by the inter-model difference in simulated changes under global warming rather than by the inter-model difference in present-day simulations. Averaged over large spatial domains, RH is approximately constant under climate change and on inter-annual time scales in most models and observations, even though regional RH variations are substantial and highly inhomogeneous. Future tropical q_{sat} rates are consistent with the current tropical q_{sat} rates, thus the inter-annual variability in tropical-averaged tropospheric q_{sat} could be representative of future changes. This offers a powerful constraint on tropical tropospheric temperature variations under climate change. However, future global q_{sat} rates are generally higher than the current global q_{sat} rates at upper and middle troposphere. Biases may be introduced when the interannual variations of global-averaged tropospheric temperature are used to represent its long-term changes.

Interestingly, the rates of water vapor increase with surface warming in response to future climate change and present-day interannual variabilities have a systematic offset. Averaged over the tropics, future rates are about 5 % higher than current rates in all models, suggesting the pattern of surface warming and the associated large-scale circulation change could be important to the averaged water vapor changes. The inter-model differences in the water vapor increase per degree of surface warming are correlated between future climate change and interannual variability, although it is not a one-to-one relationship between future and current rates. Therefore, the observed present-day interannual variation of water vapor changes could be useful to constrain the differences in future water vapor changes; however, the exact magnitude of long-term water vapor change may deviate from the interannual variation given the roles of various factors such as the direct response to forcings, the patterns of surface warming and interaction with large-scale circulation. On the inter-annual time scales, the inter-model differences in water vapor change are dominated by the inter-model differences in simulated RH change, while the model differences in temperature change drive most of the differences in water vapor sensitivity under long-term climate change. For model improvements, it is important to identify the dominant physical processes for the model discrepancy on different time scales.

Acknowledgments The authors appreciate the funding support by NASA ROSES AST, NEWS, MAP and NDOA programs. We are also grateful to Mark Richardson and two anonymous reviewers for their valuable comments. This work is performed at the Jet Propulsion Laboratory, California Institute of Technology, under contract with NASA.

References

- de Forster PMF, Collins M (2004) Quantifying the water vapour feedback associated with post-Pinatubo global cooling. *Clim Dyn* 23:207–214
- Dessler AE, Zhang Z, Yang P (2008) Water-vapor climate feedback inferred from climate fluctuations, 2003–2008. *Geophys Res Lett* 35:L20704. doi:[10.1029/2008GL035333](https://doi.org/10.1029/2008GL035333)
- Dessler AE, Sherwood SC (2009) A matter of humidity. *Science* 323:1020–1021
- Dessler AE, Wong S (2009) Estimates of the water vapor climate feedback during El Niño-Southern oscillation. *J Clim* 22:6404–6412. doi:[10.1175/2009JCLI3052.1](https://doi.org/10.1175/2009JCLI3052.1)
- Fasullo JT, Trenberth KE (2012) A less cloudy future: the role of subtropical subsidence in climate sensitivity. *Science* 338:792–794
- Fueglistaler S, Dessler AE, Dunkerton TJ, Folkins I, Fu Q, Mote PW (2009) Tropical tropopause layer. *Rev. Geophys.* 47:RG1004. doi:[10.1029/2008RG000267](https://doi.org/10.1029/2008RG000267)
- Goody RM, Yung YL (1989) Atmospheric radiation: theoretical basis, 2nd ed. Oxford University Press, p 519
- Jiang JH, Su H, Zhai C, Perun VS, Del Genio A, Nazarenko LS, Donner LJ, Horowitz L, Seman C, Cole J, Gettelman A, Ringer M, Rotstayn L, Jeffrey S, Wu T, Brent F, Dufresne J-L, Kawai H, Koshiro T, Watanabe M, LéCuyer TS, Volodin EM, Iversen T, Drange H, Mesquita MS, Read WG, Waters JW, Tian B, Teixeira J, Stephens GL (2012) Evaluation of cloud and water vapor simulations in CMIP5 climate models using NASA A-train satellite observations. *J Geophys Res* 117, D1410, 24. doi:[10.1029/2011JD017237](https://doi.org/10.1029/2011JD017237)
- Lau WK, Kim K-M (2015) Robust Hadley Circulation changes and increasing global dryness due to CO₂ warming from CMIP5 model projections. *PNAS*, Early Edition (1–6). doi: [10.1073/pnas.1418682112](https://doi.org/10.1073/pnas.1418682112)
- Manabe S, Wetherald RT (1967) Thermal equilibrium of atmosphere with a given distribution of relative humidity. *J Atmos Sci* 24:241–259
- Meinshausen M et al (2011) The RCP greenhouse gas concentrations and their extension from 1765 to 2300. *Clim Change* 109:213–241. doi:[10.1007/s10584-011-0156-z](https://doi.org/10.1007/s10584-011-0156-z)
- Minschwaner K, Dessler AE (2004) Water vapor feedback in the tropical upper troposphere: Model results and observations. *J Clim* 17:1272–1282
- Ramaswamy V, Schwarzkopf MD, Randel WJ, Santer BD, Soden BJ, Stenchikov G (2006) Anthropogenic and natural influences in the evolution of lower stratospheric cooling. *Science* 311:1138–1141
- Randall DA et al (2007) Climate models and their evaluation. In: Solomon S et al (eds) Climate change 2007: the physical science basis. Contributions of working group I to the fourth assessment report of the intergovernmental panel on climate change. Cambridge University Press, Cambridge, UK, pp 591–662
- Sherwood SC, Bony S, Dufresne J-L (2014) Spread in model climate sensitivity traced to atmospheric convective mixing. *Nature* 505:37–42. doi:[10.1038/nature12829](https://doi.org/10.1038/nature12829)
- Soden BJ, Held IM (2006) An assessment of climate feedbacks in coupled ocean-atmosphere models. *J Clim* 19:3354–3360
- Soden BJ, Held IM, Colman R, Shell KM, Kiehl JT, Shields CA (2008) Quantifying climate feedbacks using radiative kernels. *J Clim* 21:3504–3520
- Soden BJ, Jackson DL, Ramaswamy V, Schwarzkopf MD, Huang X (2005) The radiative signature of upper tropospheric moistening. *Science*. doi:[10.1126/science.1115602](https://doi.org/10.1126/science.1115602)
- Su H, Jiang JH, Zhai C, Shen TJ, Neelin JD, Stephens GL, Yung YL (2014) Weakening and strengthening structures in the Hadley Circulation change under global warming and implications for

- cloud response and climate sensitivity. *J Geophys Res Atmos* 119:5787–5805. doi:[10.1002/2014JD021642](https://doi.org/10.1002/2014JD021642)
- Takahashi H, Su H, Jiang JH (2015) Error analysis of upper tropospheric water vapor in CMIP5 models using “A-Train” satellite observations and reanalysis data. *Clim Dyn.* doi:[10.1007/s00382-015-2732-9](https://doi.org/10.1007/s00382-015-2732-9)
- Taylor KE, Stouffer RJ, Meehl GA (2012) An overview of CMIP5 and the experiment design. *Bull Am Meteorol Soc* 93:485–498. doi:[10.1175/BAMS-D-11-00094.1](https://doi.org/10.1175/BAMS-D-11-00094.1)
- Tian BJ (2015) Spread of model climate sensitivity linked to double-intertropical convergence zone bias. *Geophys Res Lett.* doi:[10.1002/2015GL064119](https://doi.org/10.1002/2015GL064119)
- Udelhofen PM, Hartmann DL (1995) Influence of tropical cloud systems on the relative humidity in the upper troposphere. *J Geophys Res* 100. doi:[10.1029/94JD02826](https://doi.org/10.1029/94JD02826)
- Vial J, Dufresne J-L, Bony S (2013) On the interpretation of inter-model spread in CMIP5 climate sensitivity estimates. *Clim Dyn* 41:3339–3362. doi:[10.1007/s00382-013-1725-9](https://doi.org/10.1007/s00382-013-1725-9)
- Zhai C, Jiang JH, Su H (2015) Long term cloud change imprinted in seasonal cloud variation: more evidence of high climate sensitivity. *Geophys Res Lett* 42:8729–8737. doi:[10.1002/2015GL065911](https://doi.org/10.1002/2015GL065911)